CHEMICAL PHYSICS

Approaching the forbidden fruit of reaction dynamics: Aiming reagent at selected impact parameters

Kelvin Anggara*, Lydie Leung*, Matthew J. Timm*, Zhixin Hu†, John C. Polanyi‡

Collision geometry is central to reaction dynamics. An important variable in collision geometry is the miss-distance between molecules, known as the "impact parameter." This is averaged in gas-phase molecular beam studies. By aligning molecules on a surface prior to electron-induced dissociation, we select impact parameters in subsequent inelastic collisions. Surface-collimated "projectile" molecules, difluorocarbene (CF_2), were aimed at stationary "target" molecules characterized by scanning tunneling microscopy (STM), with the observed scattering interpreted by computational molecular dynamics. Selection of impact parameters showed that head-on collisions favored bimolecular reaction, whereas glancing collisions led only to momentum transfer. These collimated projectiles could be aimed at the wide variety of adsorbed targets identifiable by STM, with the selected impact parameter assisting in the identification of the collision geometry required for reaction.

INTRODUCTION

Molecular motion in the course of bimolecular chemical reactions depends on collision energy and collision geometry (*1*–*3*). Measurement of impact parameter, an important variable in collision geometry, poses a long-standing problem since the incoming species, in general, randomly misses the target's center of mass. In an insightful analysis of reaction pathways, Herschbach *et al.* characterized the task of measuring the impact parameter as the pursuit of the "forbidden fruit" of reaction dynamics (*4*, *5*). Here, we undo the averaging for surface reaction by aiming an incoming "projectile" molecule with subatomic precision at the "target" molecule, by the novel means of using the rows of substrate atoms as a collimator for the projectile. The importance of the impact parameter is evident even for the case of billiards, where a head-on collision leads to a very different outcome from a glancing one.

Valuable information concerning this parameter has previously been obtained, a posteriori, from measurement of the magnitude and planarity of the rotational motion in gaseous reaction products (*6*). Impact parameter has been restricted in reactive events by photoinduced or electron-induced reaction within van der Waals complexes (*7*) or in surface-aligned reaction (SAR) (*8*–*16*) and time-resolved SAR (*9*, *17*). In these cases, the impact parameter is set by the relative alignment of the adjacent molecules, constituting the donor and acceptor of a recoiling radical that stems from bond breaking in the donor molecule. However, retention of collision energy and direction in this recoiling radical requires that the donor molecule be placed in close proximity to the acceptor, precluding variation in impact parameter. The ability to vary the impact parameter has awaited the development of a means to accelerate an adsorbed reagent over long distances in a selected direction, but with differing collision impact parameters toward the molecule under attack.

Here, the accelerated reagent projectile, difluorocarbene (CF_2), comes from electron-induced dissociation of chemisorbed trifluoromethyl (CF_3) on Cu(110) at 4.6 K. Crucially, CF_2 retains excess energy while being collimated at the surface by successive bonding to the atoms of the underlying copper row. This recoiling "hot" CF_2 can then collide at selected impact parameters with a cold chemisorbed target CF_2 or I atom, whose position and geometry have been established by scanning tunneling microscopy (STM). Our findings are that for a zero impact parameter and sufficient collision energy the bimolecular reaction $CF_2 + CF_2 = C_2F_4$ occurs, whereas for greater impact parameters, the collision geometry precludes reaction.

RESULTS AND DISCUSSION

The products of the electron-induced dissociation of CF_3 are chemisorbed CF_2 found at distances ranging as far as 50 Å from the CF_3

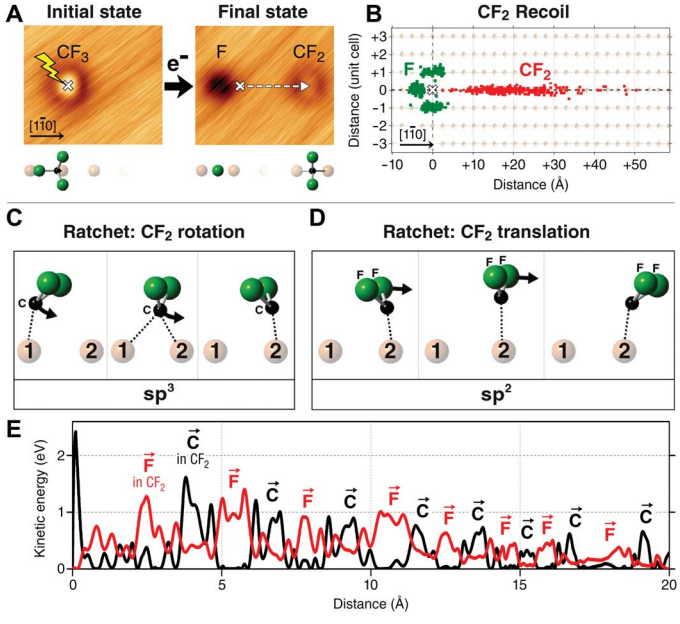

Fig. 1. Generation of CF_2 projectile from the electron-induced dissociation of CF_3. (**A**) STM images showing the initial and final states of CF_3 dissociation. The tip was placed above the CF_3 (white cross) to induce dissociation. The white arrow indicates the recoil direction of the CF_2. (**B**) Distance distribution of CF_2 (red squares) and F atom (green squares) along the [1$\bar{1}$0] direction (*x* axis) and the [001] direction (*y* axis; 1 unit cell = 3.61 Å). (**C**) CF_2 rotation in CF_2 ratcheting. (**D**) CF_2 translation in CF_2 ratcheting. (**E**) Alternating kinetic energy of F and C atoms in the ratcheting CF_2, obtained from the trajectory in fig. S1 and movie S1.

Lash Miller Chemical Laboratories, Department of Chemistry and Institute of Optical Sciences, University of Toronto, 80 St. George Street, Toronto, Ontario M5S 3H6, Canada.
*These authors contributed equally to this work.
†Present address: Center for Joint Quantum Studies and Department of Physics, Tianjin University, Tianjin 300350, China.
‡Corresponding author. Email: jpolanyi@chem.utoronto.ca

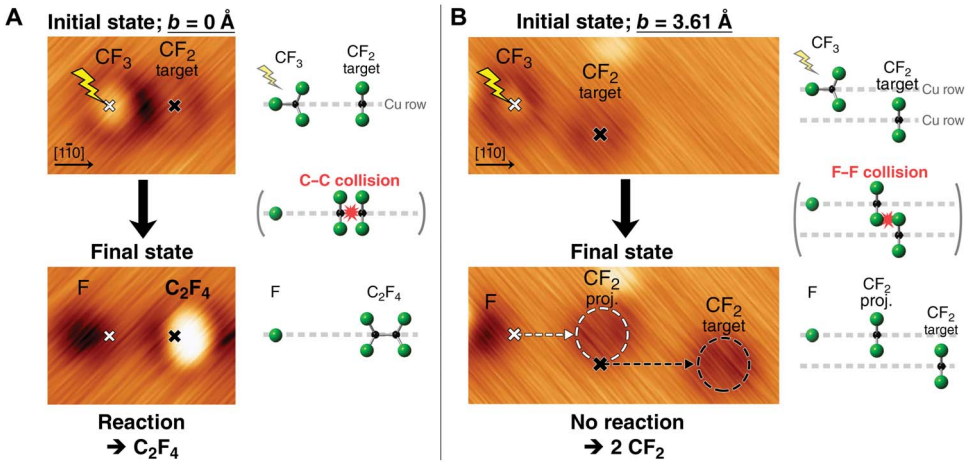

Fig. 2. Effects of different impact parameters, *b*, on CF_2 + CF_2 collision. (**A**) STM images and schematics showing the initial and final states of *b* = 0 collision. (**B**) Same data for *b* = 3.61 Å collision. In both panels, the tip was placed above the CF_3 (white cross) to produce the CF_2 projectile. The black cross marks the initial position of the CF_2 target. In the final state for *b* = 3.61 Å, the dashed circles indicate the new positions of the CF_2 projectile and CF_2 target (white and black circles, respectively) after the collision.

along the [1$\bar{1}$0] direction (see Fig. 1, A and B); the second product of dissociation is a F atom, which recoils only one lattice space. This short recoil of the F atom, as opposed to the long recoil of CF_2, is attributable to the strong binding of F to the surface, computed to be 5.0 eV, as compared to that of CF_2, computed as 1.9 eV. The CF_2 is found to be sharply collimated to a single Cu row, with a measured spread of only ±1° (Fig. 1B). This directionality is present in all the 336 of the CF_2 recoil events examined. Density functional theory (DFT) calculations of the adsorbed CF_3 shows a bond extension of 0.07 Å for the C–F bond along the [1$\bar{1}$0]; this is consistent with weakening of the C–F bond that is found to break.

Molecular dynamics (MD) calculations using the "Impulsive Two-State" (I2S) model (*18*–*20*) account for the observed long-range recoil of the chemisorbed CF_2 product (see Supplementary Text). These dynamics (fig. S1) led to a calculated CF_2 travel distance of 21.6 Å, comparable with the observed recoil that averaged 19.7 ± 8.0 Å. The recoil calculated in the I2S model was due to the C–F repulsion in the anionic state of CF_3. Upon returning to the ground state, the CF_2 and the F atom recoil in opposite directions.

The sustained long-range motion of the chemisorbed CF_2, initiated by the repulsion described above, took place through multiple alternating motions resembling a ratchet. This "ratcheting" (see Fig. 1, C and D) comprised frustrated rotation followed by frustrated translation, the latter producing the largest center-of-mass displacement along the copper row. Efficient rotation-translation coupling has previously been proposed in theoretical studies of migration dynamics (*21*) and in laser-induced CO migration (*22*, *23*).

The CF_2 ratcheting is shown in Fig. 1 (C and D) and movie S1. The dynamics of the alternating motion involve CF_2 partial rotation, which displaces its C atom by 2.55 Å from a Cu atom toward the adjacent Cu atom of the same row (see Fig. 1C). The breaking of the old C–Cu bond causes the Cu atom left behind by the CF_2 to rise as much as 0.4 Å. This resembles the "walking" of a divalent C atom of CH_2 migrating by alternate bonding to Cu atoms of a pair of rows (*20*). Here, it is due to successive binding of the sp^3-hybridized C atom to adjacent Cu atoms of a single row.

Following partial rotation, the singly bound CF_2-Cu behaves as if sp^2-hybridized, with a p orbital inducing the tilt of the CF_2 plane that propels the F atoms forward. Since the F atoms are at the center of mass

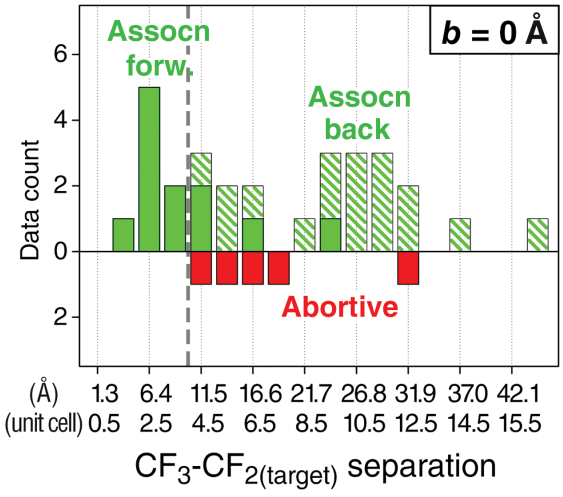

Fig. 3. Effects of different initial projectile-target separation on zero–impact parameter CF_2 + CF_2 collision. The dashed line at ~11 Å demarcates the regime with 100% reaction probability (high CF_2 + CF_2 collision energy) from that with mixed outcomes (low collision energy). The stacked histogram plot uses a bin size of 2.55 Å (1 unit cell along the [1$\bar{1}$0] direction). Assocn means association.

of CF_2, the resulting motion resembles frustrated translation (Fig. 1D). The ratcheting is seen in Fig. 1E to embody the alternating motion of the C and the F atoms, carrying the chemisorbed CF_2 along the single Cu row. Facile energy transfer between rotation and translation permits these motions to dominate energy dissipation to the surface (fig. S2). Thereafter, the CF_2 retains sufficient energy to have reactive or other inelastic encounters of a known impact parameter.

We have studied encounters between the CF_2 projectile and a stationary target, chemisorbed CF_2, and, later in the text, chemisorbed I atom. Since the CF_2 projectile recoil is collimated along [1$\bar{1}$0], the perpendicular distance along [001] becomes the collision impact parameter (*b*). The distance along [1$\bar{1}$0], denoted as *d*, governs the collision energy since the CF_2 cools as it travels (Fig. 1E and fig. S2). The lower the value of *d*, the higher the projectile energy in a subsequent collision (see fig. S2).

The principal finding of this work is that association reaction between the CF_2 projectile and the CF_2 target occurs at zero impact parameter, $b = 0$, but not at $b \geq 3.61$ Å, at comparable d values and hence comparable collision energies. We obtain the contrasting impact parameters by having the projectile and target on the same row for $b = 0$ or on adjacent Cu rows for $b = 3.61$ Å (see Fig. 2). For $b = 0$, experimentally, the CF_2 projectile collides with the CF_2 target to produce a bright oval feature on the surface. This new feature is confirmed to be a single molecule by its intact electron-induced diffusion. The feature is identified as chemisorbed C_2F_4 by STM simulation (see fig. S3). The formation of C_2F_4 is due to the association reaction between projectile and target in 29 cases out of 34 of zero impact parameter collision, $CF_2 + CF_2$.

For impact parameter $b = 3.61$ Å, with CF_2 projectile and target on adjacent rows, no C_2F_4 adduct is observed in all five cases that showed inelastic encounters. These nonreactive cases involve a CF_2 projectile with recoil distance d as small as 1.3 Å, hence the highest achievable collision energy. As shown in Fig. 2B, the projectile travels along the [1$\bar{1}$0] Cu row, and following the inelastic encounter, the previously cold target moves in the same direction along its adjacent Cu row. It is noteworthy that collision between the CF_2 projectile and CF_2 target causes the target to recoil despite the large impact parameter of 3.61 Å, surmounting a computed 0.3-eV diffusion barrier. This long-range repulsion between the two CF_2 is to be expected, given the diameter of saturated fluorocarbons, for example, carbon tetrafluoride with a diameter of 4.7 Å, obtained from transport properties (*24*).

A qualitatively similar momentum transfer is observed for the CF_2 projectile colliding with a chemisorbed I atom at an impact parameter $b = 1.80$ Å (fig. S4). The inelastic collision between the CF_2 projectile and the I atom is observed to move the I atom one lattice spacing surmounting a diffusion energy barrier of 0.1 eV.

We further investigate reactive collisions between the CF_2 projectile and the CF_2 target with zero impact parameter to experimentally form C_2F_4 for different projectile energies. This is done by examining the effect on the observed dynamics of varying the distance, d, between

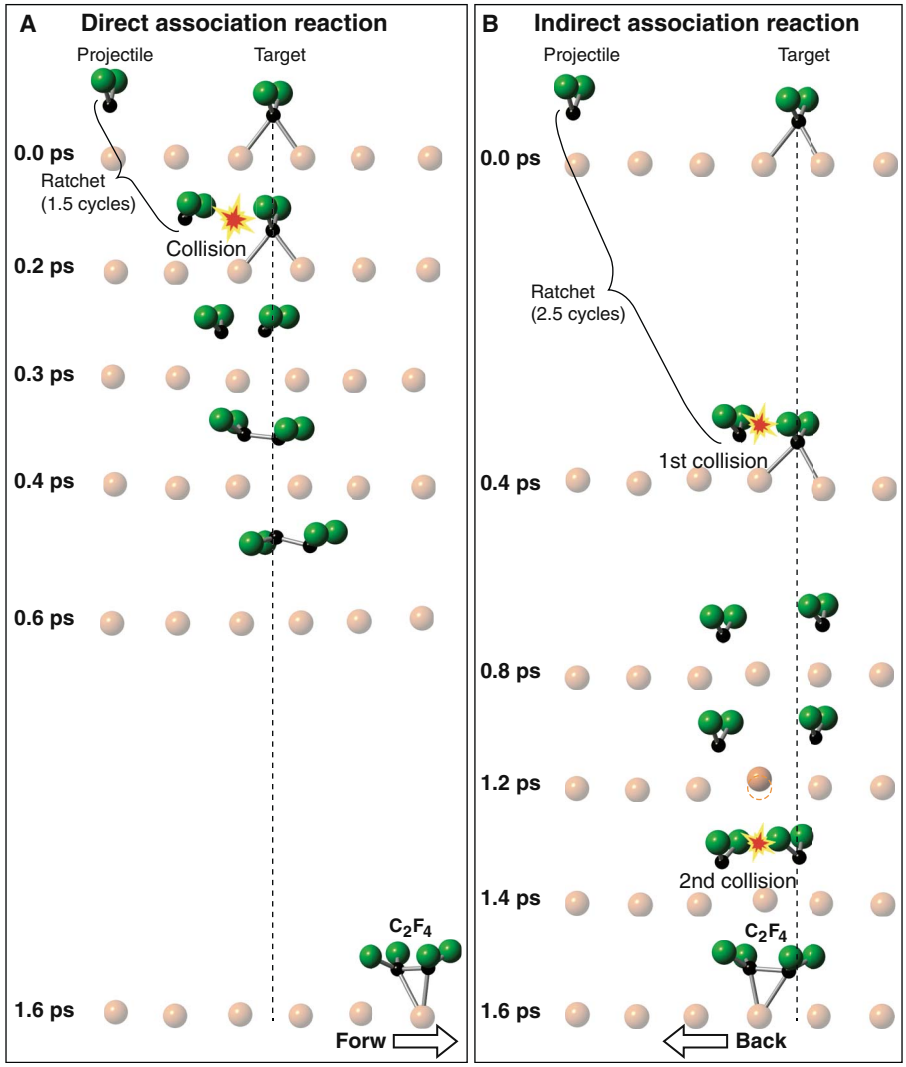

Fig. 4. Computed dynamics for "direct" and "indirect" association reactions. (**A**) Trajectory for direct single-collision reaction giving the forward-scattered C_2F_4 product at 1.5-eV collision energy. (**B**) Trajectory for indirect double-collision reaction giving the backward-scattered C_2F_4 product at 1.2-eV collision energy. In both panels, the vertical dashed lines indicate the initial position of the CF_2 target. Here, a collision is said to occur when both CF_2 have reached their closest-approach distance of 2.55 Å, 1 unit cell along the [1$\bar{1}$0] direction (whether the first or the second collision).

the CF_3 parent and the CF_2 target. As shown in Fig. 3, we examined a total of 34 cases. For small *d*, <11 Å, corresponding to higher projectile energies, all cases give forward scattering of the C_2F_4 product, along the continuation of the direction of the projectile. For higher *d*, >11 Å, hence lower projectile energies, the majority of cases (66 %) gives backward scattering of C_2F_4. In addition, lower collision energy gives rise to a small number of abortive outcomes (19%) and to a minor percentage of forward-scattered product, C_2F_4 (15%). The abortive outcome denotes a nonreactive event (fig. S5). The observation of forward scattering at increased collision energy and backward scattering at lowered collision energy, measurable here for the first time at a single impact parameter, conforms to the results from MD calculations at selected impact parameters described below.

We performed the MD calculations for $b = 0$ and $b = 3.61$ Å. The observation of reaction at $b = 0$ and no reaction at $b = 3.61$ Å is explained by the differing geometries in the $CF_2 + CF_2$ collisions at the two impact parameters. MD calculations for $b = 3.61$ Å show F–F repulsion between the projectile and the target, with no reaction. By contrast, calculations for $b = 0$ lead to association reaction due to C–C collision, as in Fig. 4. MD gives forward-scattered C_2F_4 at a higher collision energy of 1.5 eV and backward-scattered C_2F_4 at a lower collision energy of 1.2 eV. In the course of reaction, the two reagents are seen to rotate toward each other to form the C–C bond. At a low collision energy of 0.7 eV, insufficient projectile rotation prevented C–C bond formation.

The forward trajectory shows the projectile momentum transferred to the C_2F_4 product, which retains its direction of travel (see Fig. 4A and movie S2). The forward-scattered C_2F_4 is the product of a direct association with a single encounter between the CF_2 reagents, which overcome a computed barrier of 0.6 eV (shown in fig. S6).

The backward trajectory gives reaction by way of an indirect reactive encounter involving two successive collisions (see Fig. 4B and movie S3). The first collision results in momentum transfer between the projectile, target, and surface but no C–C bond formation. Following 1.2 ps, projectile and target CF_2 interact with a single raised Cu atom, which catalyzes a second collision. The second collision surmounts the computed 0.4-eV barrier (shown in fig. S7) to give C–C bond formation and backward-scattered C_2F_4. The raised Cu atom, present in this indirect reaction, but not in the direct, alters the reaction pathway, giving a lower barrier indicative of a catalytic effect.

CONCLUSION

Using STM, we have shown that a recoiling biradical, termed the projectile, can exhibit sharply collimated motion along a row of substrate copper atoms. The resulting observed "surface molecular beam" of chemisorbed CF_2 was aimed with selected impact parameters at coadsorbed target collision partners. The collision with a second chemisorbed CF_2 was shown to exhibit predominantly reaction at zero impact parameter, changing to nonreactive inelastic encounters for intermediate impact parameters. The study of bimolecular collisions between projectile and target adsorbates at a surface, using selected collision impact parameters, should, in the future, lead to improved understanding of the molecular mechanisms underlying surface-catalyzed reaction.

MATERIALS AND METHODS

Experiment

Experiments were conducted using a low-temperature scanning tunneling microscope (Omicron) in an ultrahigh vacuum chamber with base pressure $<3.0 \times 10^{-11}$ mbar. The Cu(110) surface was prepared by repeated cycles of sputtering by Ar^+ (0.6 keV) and annealing (800 K) until a clean surface was observed by STM. To generate CF_3 on the surface, trifluoroiodomethane (CF_3I; SynQuest; purity, 99%) was dosed onto the copper surface via a capillary tube. The sample temperature rose up to ~14 K during the dose. The CF_3I was found to dissociate upon adsorption to give chemisorbed CF_3 and I atoms on the surface.

All STM images were taken at 4.6 K using constant current mode. The bias reported refers to the sample bias. The STM images were obtained at a bias of −0.05 V and a current of 0.05 nA. The C–F bond breaking of CF_3 was induced by (i) placing the tip over the adsorbate, (ii) adjusting the tip height, (iii) turning off the feedback loop, and (iv) ramping up the sample bias to V_{pulse}. A single discontinuity observed in the tunneling current recorded against time indicated that an event had occurred underneath the tip. The reaction was confirmed by the imaging of the reaction products in a subsequent scan. The distance and direction of the product fragments were analyzed using the WSxM software (*25*).

To establish the number of electrons required in the dissociation of CF_3, the reaction rate was measured as a function of tunneling current following a previously established method (*26*, *27*). For a chosen tunneling current, the time prior to the discontinuity in the current-versus-time curve was plotted as a histogram whose bin size was set by Doane's formula (*28*). By fitting a single-parameter exponential function (e^{-Rt}) to the normalized histogram, the decay constant (*R*), which was the average reaction rate, and its fitting error were obtained. Only cases with a single discontinuity were considered.

Theory

Plane-wave DFT calculations were conducted using the Vienna Ab initio Simulation Package (VASP 5.4.1) (*29*, *30*) at SciNet supercomputer (*31*). The calculations used the projector augmented wave method (*32*, *33*), Perdew-Burke-Ernzerhof functional (*34*), and Grimme's semiempirical dispersion correction (DFT-D3) (*35*). The energy cutoff for the plane-wave basis set was 400 eV. The surface was modeled by a slab consisting of five layers of Cu atoms separated by 17 Å of vacuum layer. All atoms were allowed to move, except the bottom two layers of Cu atoms. The relaxation, projected density of state (pDOS), and climbing image nudged elastic band (CI-NEB) calculations were conducted on a (4×6) slab, whereas the MD calculations were conducted on a (3×8) slab. The relaxation, pDOS, CI-NEB, and MD calculations used a single Γ-point *k*-mesh sampling. In the relaxation calculation, the system was relaxed until the force on each atom was less than 0.01 eV/Å. In the pDOS calculation, Gaussian smearing ($\sigma = 0.25$ eV) was used. In the MD calculations, a time step of 0.5 fs was used under the microcanonical condition. At the start of the MD, the initial state was initialized by random velocities sampled from the Boltzmann distribution at 4.7 K. Molecular structures presented were visualized using the VESTA software (*36*).

STM simulations were used to identify the species observed on the surface (see fig. S3); the calculation was performed using the Tersoff-Hamann approximation (*37*) and visualized using the Hive software (*38*, *39*).

CI-NEB (*40*) was used to obtain the diffusion barrier of chemisorbed CF_2 and I atom along the Cu row direction. Five images were used in both cases. The calculations were conducted until the forces orthogonal to the band were less than 0.02 eV/Å.

The electron-induced dissociation of CF_3 was simulated using the I2S model (*18*–*20*) implemented in the MD calculations. The C–F

repulsion caused by electron attachment to the CF_3 molecule was modeled by the anionic pseudopotential method (*41*, *42*). The anionic potential energy surface (pes*) for CF_3 was constructed by exciting one 1s electron of the F atom in the C–F bond directed along the Cu row to its valence 2p orbital, giving a pseudo-ionic configuration [He] $2s^2\ 2p^6$. The reaction trajectory was obtained by evolving the system on the pes* for a short period of time (t^*) and, afterward, with a retention of positions and momenta, on the ground pes until the system settled in a potential well.

The MD trajectories for association reactions were obtained by introducing a relaxed, stationary CF_2 target into the path of CF_2 projectile obtained from the CF_3 I2S dynamics at 179 fs. The direct MD trajectory was obtained by placing the CF_2 target on a short-bridge site 3.5 unit cells (8.93 Å) away from the CF_3 position. The indirect MD trajectory was obtained by placing the CF_2 target on a short-bridge site 4.5 unit cells (11.47 Å) away from the CF_3 position. The collision energy of 1.5 eV in the forward trajectory and 1.2 eV in the backward trajectory is the sum of rotational and translational energies of the CF_2 projectile when both CF_2 are at their closest-approach distances of 2.55 Å (1 unit cell).

SUPPLEMENTARY MATERIALS

Supplementary material for this article is available at http://advances.sciencemag.org/cgi/content/full/4/10/eaau2821/DC1

Supplementary Text

Fig. S1. Computed dynamics for the electron-induced reaction of CF_3, obtained from the I2S model.

Fig. S2. Distance dependence of the energy in the recoiling CF_2.

Fig. S3. Identification of molecular species on the surface.

Fig. S4. CF_2 + I collision at 1.80 Å impact parameter, giving only momentum transfer from the projectile to the target.

Fig. S5. Nonreactive outcome of a zero–impact parameter CF_2 + CF_2 collision, resulting in only momentum transfer from the projectile to the target.

Fig. S6. Trajectory for direct association reaction superimposed on a restricted cut through the ground potential energy surface.

Fig. S7. Trajectory for indirect association reaction superimposed on a restricted cut through the ground potential energy surface.

Fig. S8. Evidence for electron-induced reaction.

Movie S1. Computed dynamics for the electron-induced reaction of CF_3, obtained from the I2S model.

Movie S2. Computed dynamics for direct reaction.

Movie S3. Computed dynamics for indirect reaction.

REFERENCES AND NOTES

1. D. R. Herschbach, Molecular dynamics of elementary chemical reactions (Nobel lecture). *Angew. Chem. Int. Ed. Engl.* **26**, 1221–1243 (1987).
2. Y. T. Lee, Molecular beam studies of elementary chemical processes (Nobel lecture). *Angew. Chem. Int. Ed. Engl.* **26**, 939–951 (1987).
3. R. D. Levine, *Molecular Reaction Dynamics* (Cambridge Univ. Press, 2005).
4. D. Herschbach, Chemical stereodynamics: Retrospect and prospect. *Eur. Phys. J. D* **38**, 3–13 (2006).
5. H. Pan, K. Liu, A. Caracciolo, P. Casavecchia, Crossed beam polyatomic reaction dynamics: Recent advances and new insights. *Chem. Soc. Rev.* **46**, 7517–7547 (2017).
6. K. S. Kalogerakis, R. N. Zare, Energy and angular momentum control of the specific opacity functions in the Ba+HI→BaI+H reaction. *J. Chem. Phys.* **104**, 7947–7964 (1996).
7. S. Buelow, G. Radhakrishnan, J. Catanzarite, C. Wittig, The use of van der Waals forces to orient chemical reactants: The H+CO_2 reaction. *J. Chem. Phys.* **83**, 444–445 (1985).
8. E. B. D. Bourdon, P. Das, I. Harrison, J. C. Polanyi, J. Segner, C. D. Stanners, R. J. Williams, P. A. Young, Photodissociation, photoreaction and photodesorption of adsorbed species. Part 2. CH_3Br and H_2S on LiF(001). *Faraday Discuss. Chem. Soc.* **82**, 343–358 (1986).
9. J. C. Polanyi, A. H. Zewail, Direct observation of the transition state. *Acc. Chem. Res.* **28**, 119–132 (1995).
10. C. E. Tripa, J. T. Yates Jr., Surface-aligned reaction of photogenerated oxygen atoms with carbon monoxide targets. *Nature* **398**, 591–593 (1999).
11. L. J. Lauhon, W. Ho, The initiation and characterization of single bimolecular reactions with a scanning tunneling microscope. *Faraday Discuss.* **117**, 249–255 (2000).
12. S. W. Hla, L. Bartels, G. Meyer, K.-H. Rieder, Inducing all steps of a chemical reaction with the scanning tunneling microscope tip: Towards single molecule engineering. *Phys. Rev. Lett.* **85**, 2777–2780 (2000).
13. P. Maksymovych, D. C. Sorescu, K. D. Jordan, J. T. Yates Jr., Collective reactivity of molecular chains self-assembled on a surface. *Science* **322**, 1664–1667 (2008).
14. T. Kumagai, A. Shiotari, H. Okuyama, S. Hatta, T. Aruga, I. Hamada, T. Frederiksen, H. Ueba, H-atom relay reactions in real space. *Nat. Mater.* **11**, 167–172 (2011).
15. Z. Ning, J. C. Polanyi, Surface aligned reaction. *J. Chem. Phys.* **137**, 91706 (2012).
16. Z. Ning, J. C. Polanyi, Charge delocalization induces reaction in molecular chains at a surface. *Angew. Chem. Int. Ed. Engl.* **52**, 320–324 (2013).
17. M. E. Vaida, T. M. Bernhardt, in *Ultrafast Phenomena in Molecular Sciences*, R. de Nalda, L. Bañares, Eds. (Springer International Publishing, 2014), pp. 231–261.
18. L. Leung, T. Lim, Z. Ning, J. C. Polanyi, Localized reaction at a smooth metal surface: *p*-Diiodobenzene at Cu(110). *J. Am. Chem. Soc.* **134**, 9320–9326 (2012).
19. A. Eisenstein, L. Leung, T. Lim, Z. Ning, J. C. Polanyi, Reaction dynamics at a metal surface; halogenation of Cu(110). *Faraday Discuss.* **157**, 337–353 (2012).
20. A. Chatterjee, F. Cheng, L. Leung, M. Luo, Z. Ning, J. C. Polanyi, Molecular dynamics of the electron-induced reaction of diiodomethane on Cu(110). *J. Phys. Chem. C* **118**, 25525–25533 (2014).
21. K. D. Dobbs, D. J. Doren, Dynamics of molecular surface diffusion: Origins and consequences of long jumps. *J. Chem. Phys.* **97**, 3722–3735 (1992).
22. E. H. G. Backus, A. Eichler, A. W. Kleyn, M. Bonn, Real-time observation of molecular motion on a surface. *Science* **310**, 1790–1793 (2005).
23. H. Ueba, B. N. J. Persson, Heating of adsorbate by vibrational-mode coupling. *Phys. Rev. B* **77**, 035413 (2008).
24. J. O. Hirschfelder, C. F. Curtiss, R. B. Bird, *Molecular Theory of Gases and Liquids* (Wiley, 1954).
25. I. Horcas, R. Fernández, J. M. Gómez-Rodríguez, J. Colchero, J. Gómez-Herrero, A. M. Baro, WSXM: A software for scanning probe microscopy and a tool for nanotechnology. *Rev. Sci. Instrum.* **78**, 013705 (2007).
26. W. Ho, Single-molecule chemistry. *J. Chem. Phys.* **117**, 11033 (2002).
27. D. Riedel, Single molecule manipulation at low temperature and laser scanning tunnelling photo-induced processes analysis through time-resolved studies. *J. Phys. Condens. Matter* **22**, 264009 (2010).
28. D. P. Doane, Aesthetic frequency classifications. *Am. Stat.* **30**, 181–183 (1976).
29. G. Kresse, J. Hafner, Ab initio molecular dynamics for liquid metals. *Phys. Rev. B* **47**, 558–561 (1993).
30. G. Kresse, J. Furthmüller, Efficient iterative schemes for ab initio total-energy calculations using a plane-wave basis set. *Phys. Rev. B* **54**, 11169–11186 (1996).
31. C. Loken, D. Gruner, L. Groer, R. Peltier, N. Bunn, M. Craig, T. Henriques, J. Dempsey, C.-H. Yu, J. Chen, J. L. Dursi, J. Chong, S. Northrup, J. Pinto, N. Knecht, R. Van Zon, SciNet: Lessons learned from building a power-efficient top-20 system and data centre. *J. Phys. Conf. Ser.* **256**, 12026 (2010).
32. P. E. Blöchl, Projector augmented-wave method. *Phys. Rev. B* **50**, 17953–17979 (1994).
33. G. Kresse, D. Joubert, From ultrasoft pseudopotentials to the projector augmented-wave method. *Phys. Rev. B* **59**, 1758–1775 (1999).
34. J. P. Perdew, K. Burke, M. Ernzerhof, Generalized gradient approximation made simple. *Phys. Rev. Lett.* **77**, 3865–3868 (1996).
35. S. Grimme, J. Antony, S. Ehrlich, H. Krieg, A consistent and accurate ab initio parametrization of density functional dispersion correction (DFT-D) for the 94 elements H-Pu. *J. Chem. Phys.* **132**, 154104 (2010).
36. K. Momma, F. Izumi, VESTA3 for three-dimensional visualization of crystal, volumetric and morphology data. *J. Appl. Crystallogr.* **44**, 1272–1276 (2011).
37. J. Tersoff, D. R. Hamann, Theory of the scanning tunneling microscope. *Phys. Rev. B* **31**, 805–813 (1985).
38. D. Vanpoucke, *HIVE STM-program » The Delocalized Physicist*; http://dannyvanpoucke.be/hive-stm-en/ [accessed 9 August 2018].
39. D. E. P. Vanpoucke, G. Brocks, Formation of Pt-induced Ge atomic nanowires on Pt/Ge (001): A density functional theory study. *Phys. Rev. B* **77**, 241308 (2008).
40. G. Henkelman, B. P. Uberuaga, H. Jónsson, A climbing image nudged elastic band method for finding saddle points and minimum energy paths. *J. Chem. Phys.* **113**, 9901–9904 (2000).
41. L. Köhler, G. Kresse, Density functional study of CO on Rh(111). *Phys. Rev. B* **70**, 165405 (2004).
42. W. Ji, Z.-Y. Lu, H. Gao, Electron core-hole interaction and its induced ionic structural relaxation in molecular systems under x-ray irradiation. *Phys. Rev. Lett.* **97**, 246101 (2006).

Acknowledgments
Funding: This work was funded by the Natural Sciences and Engineering Research Council of Canada (NSERC) and the University of Toronto NSERC General Research Fund. Computations were performed on the General Purpose Cluster at SciNet HPC (High Performance Computing) Consortium. SciNet is funded by the Canada Foundation for Innovation under the auspices of Compute Canada, the Government of Ontario, Ontario Research Fund–Research Excellence, and the University of Toronto. K.A. thanks the Connaught International Scholarship for Doctoral Students for financial support. **Author contributions:** J.C.P. designed and supervised the project. K.A., L.L., and M.J.T. performed the experiments. K.A. and L.L. analyzed the data. K.A. and Z.H. conducted the ab initio calculations. All the authors contributed to the manuscript. **Competing interests:** The authors declare that they have no competing interests. **Data and materials availability:** All data needed to evaluate the conclusions in the paper are present in the paper and/or the Supplementary Materials. Additional data related to this paper may be requested from the authors.

Submitted 24 May 2018
Accepted 30 August 2018
Published 5 October 2018
10.1126/sciadv.aau2821

Citation: K. Anggara, L. Leung, M. J. Timm, Z. Hu, J. C. Polanyi, Approaching the forbidden fruit of reaction dynamics: Aiming reagent at selected impact parameters. *Sci. Adv.* **4**, eaau2821 (2018).

Approaching the forbidden fruit of reaction dynamics: Aiming reagent at selected impact parameters

Kelvin Anggara, Lydie Leung, Matthew J. Timm, Zhixin Hu and John C. Polanyi

Sci Adv **4** (10), eaau2821.
DOI: 10.1126/sciadv.aau2821